Computational Study on OH and Cl Initiated Oxidation

Bull. Korean Chem. Soc. **2014**, Vol. 35, No. 5   1385

http://dx.doi.org/10.5012/bkcs.2014.35.5.1385

Computational Study on OH and Cl Initiated Oxidation of 2,2,2-Trifluoroethyl Trifluoroacetate (CF₃C(O)OCH₂CF₃)

Hari Ji Singh, * **Laxmi Tiwari, and Pradeep Kumar Rao**

*Department of Chemistry, DDU Gorakhpur University, Gorakhpur-273 009. * E-mail: hjschem50@gmail.com*
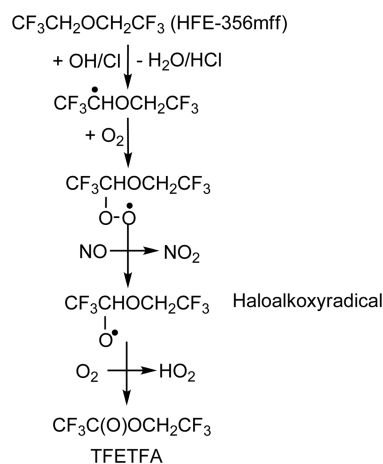
Hydrofluoroethers (HFEs) are developed as a suitable for the replacement of environmentally hazardous CFCs and are termed as third generation refrigerants. One of the major products of decomposition of HFEs in the atmosphere is a fluoroester. The present study relates to the OH and Cl initiated oxidation of CF₃C(O)OCH₂CF₃ formed from the oxidation of HFE-356mff. The latter is used as a solvent in the industry and reaches the atmosphere without any degradation. Kinetics of the titled molecule has been studied at MPWB1K/6-31+G(d,p) level of theory. Single point energy calculations have been made at G2(MP2) level of theory and barrier heights are determined. The rate constants are calculated using canonical transition state theory. Tunnelling correction are made using one-dimensional Eckart potential barrier. The rate constant calculated during the present study are compared with the experimental values determined using relative rate method and FTIR detection technique.

Key Words : Atmospheric oxidation, G2(MP2), Eckart barrier, HFEs, TFETFA

Introduction

Halons have been determined to be responsible for depletion of stratospheric ozone resulting in the global warming. These are undesirable in the atmosphere and therefore, banned globally for their use in industrial applications.[1-4] A particular category of halons, chlorofluorocarbons (CFCs) widely used in the industry are quite stable and reach as such in the stratospheric region of atmosphere. These take part in the catalytic destruction of ozone. Therefore, attention has been directed to find suitable and environmental friendly replacements. A large number of compounds such as hydrochlorofluorocarbons (HCFCs), hydrofluorocarbons (HFCs), perfluorocarbons (PFCs) and hydrofluoroethers (HFEs) have been found to have similar physical properties as that of CFCs and these may suitably be used as an alternative in many industrial applications such as refrigerants, blowing and cleaning agents. Amongst the above, hydrofluoroethers (HFEs) are mostly used as industrial solvents and cleaning agents. These possess almost zero ozone depleting potential due to absence of chlorine.[5] However, the presence of C-F bond in HFEs may enhance the strong absorption in the range 1000-3000 cm⁻¹ that may cause a potential greenhouse effect.[6,7] HFEs have ether (—O—) linkage as a result of which they are highly reactive in the upper atmospheric region. It is a known fact that the atmospheric oxidation of HFEs leads to the formation of fluorinated esters as primary products.[8-12]

In the tropospheric region highly reactive oxidants OH and Cl are abundantly present.[13] These oxidants would initiate the oxidation of HFE-356mff (CF₃CH₂OCH₂CF₃) that ultimately formed 2,2,2-trifluoroethyl trifluoroacetate (TFETFA). Various pathways involved during the oxidation of CF₃CH₂OCH₂CF₃ (HFE356mff) leading to the formation

CF₃CH₂OCH₂CF₃ (HFE-356mff)

+ OH/Cl | - H₂O/HCl

CF₃ĊHOCH₂CF₃

+ O₂

CF₃CHOCH₂CF₃
|
O-Ȯ

NO → NO₂

CF₃CHOCH₂CF₃   Haloalkoxyradical
|
Ȯ

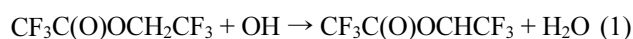O₂ → HO₂

CF₃C(O)OCH₂CF₃
TFETFA

Scheme 1. Degradation pathways of HFE-356mff leading to the formation of 2,2,2-trifluoroethyl trifluoroacetate (TFETFA).

of TFETFA are schematically shown in Scheme 1.

Studies have shown that further oxidation of FESs leads to the formation of fluorinated acetic acid and the corresponding anhydride along with CF₂O and its hydrolysis products CO₂ and HF leading to acid rains.[14-16] Therefore, it is necessary to understand the chemistry of fluorinated esters in the atmosphere in order to assess the environmental acceptability of HFEs as a plausible replacement of chlorofluorocarbons.

Therefore, it is pertinent to have an understanding of the chemistry of oxidative degradation of fluoroesters formed as a result of oxidation of HFEs. In this work we have studied the kinetics of OH and Cl initiated oxidation of TFETFA. TFETFA possess only one hydrogen and its abstraction reaction by OH and Cl are represented as:

$$CF_3C(O)OCH_2CF_3 + OH \rightarrow CF_3C(O)OCHCF_3 + H_2O \quad (1)$$

$$CF_3C(O)OCH_2CF_3 + Cl \rightarrow CF_3C(O)OCHCF_3 + HCl \quad (2)$$

Based on relative kinetic method using FT-IR detection technique Blanco *et al.*[17] derived the rate constants of the above two channels as $k_{OH} = 1.05 \pm 0.23 \times 10^{-13}$ and $k_{Cl} = 1.18 \times 10^{-15}$ cm^3 molecule^{-1} s^{-1} at 298 K and 1 atm pressure. In another study using the same technique Wallington *et al.*[18] reported the rate constant of reaction (2) to be 9.0×10^{-16} cm^3 molecule^{-1} s^{-1} However, to the best of our knowledge no theoretical studies have been done so far on the above two reactions. Thus, we found it genuine to study the kinetics of the above two reactions using high level computational methods and compare the computed values with the experimental data available in the literature.

Theoretical Details

All the electronic structure calculations were performed using GAUSSIAN 09[19] software package using the methods implemented therein. The geometries of reactants [CF$_3$C(O)-OCH$_2$CF$_3$, OH], products [CF$_3$C(O)OCHCF$_3$, H$_2$O, HCl] and transition states TS-OH and TS-Cl were optimized at DFT level using hybrid meta density functional MPWB1K with 6-31+G(d,p) basis set.[20] MPWB1K method is based on the modified Perdew and Wang exchange functional (MPW) and Becke's 1995 correlation functional (B95).[21,22] The MPWB1K method has been found to yield reliable thermo-chemical data in order to calculate the energy barrier needed for the rate constant determination.[23] The harmonic vibrational frequencies of the stationary point (reactants and products) and saddle point (transition state) and zero point energies were obtained at the same level of theory at which the optimization was made. The frequency calculation showed that all the stationary points belonged to the local minima on their potential energy surface shown by the positive vibrational frequencies. On the other hand transition states were characterized by the presence of only one imaginary frequency (NIMAG=1). Intrinsic reaction coordinate (IRC) calculation was also performed at the same level of theory by making 15 point on both (reactant and product) sides of the transition state with the step size of 0.01 amu$^{1/2}$-bohr in order to confirm that transition state connected the reactants and products smoothly.

In order to have a more reliable barrier heights, single point energy calculation were carried out at G2(MP2)[24] level using MPWB1K/6-31+G(d,p) optimized geometries of reactants, products and transition states. The zero point corrected total energy for each species was used for the determination of the energy barrier. A recommended value of scaling factor of 0.9537 was used for correcting the zero point energy.[25]

The rate constants for reaction channels 1 and 2 were calculated using the canonical transition state theory (CTST)[26] which included a semi-classical one-dimensional multiplicative tunnelling correction factor as represented by the following expression:

$$k = \Gamma(T)\frac{k_B T Q_{TS}^{\ddagger}}{h \, Q_R} \exp\left(-\frac{\Delta E_0}{RT}\right) \quad (3)$$

where $\Gamma(T)$ stands for the tunnelling correction factor at temperature T, $Q_{TS}^{\ddagger}$ and Q_R are the total partition function of transition state and reactant respectively and ΔE_0 is the activation energy. R is the universal gas constant and k_B and h are Boltzmann and Planck's constants respectively. The tunnelling correction factor $\Gamma(T)$ is defined as the ratio of the quantum mechanical to the classical mechanical barrier crossing rate. It is expressed as[27]

$$\Gamma(T) = \frac{\exp\left(\frac{V_F}{k_B T}\right)}{k_B T} \int_{E_o}^{\infty} K(E) \exp\left(-\frac{E}{k_B T}\right) dE \quad (4)$$

where V_F is the forward reaction barrier and K is the transmission probability for tunnelling which depends on E and three other parameters determined from the shape of the barrier and effective mass of the system. The Eckart[28] barrier was the first realistic barrier for which quantum mechanical solution was obtained and it is used frequently to determine the chemical rate constants. The one-dimension Eckart's potential has the form

$$V = -\frac{Ay}{1-y} - \frac{By}{(1-y)^2} \quad (5)$$

$$y = -\exp(2\pi x/L) \quad (6)$$

where x is the variable measured along the reaction coordinate and L is the characteristic length. A and B are related to the forward and reverse energy barriers and L to the second derivative of V at its maximum written as F* and these are given as

$$\begin{aligned} &A = V_F - V_R \\ &B = (\sqrt{V_F} + \sqrt{V_R})^2 \\ &L = 2\pi \, (-2/F^*)^{1/2} \, (V_F^{-1/2} + V_R^{-1/2})^{-1} \end{aligned} \quad (7)$$

Brown[29] derived expression for the calculation of the transmission probability in terms of three parameters defined by Johnston and Heicklen[30] and wrote a computer code for the evaluation of tunnelling correction factor in the case of unsymmetrical Eckart type potential barriers given by Eq. (5). In the present study we used the code and calculated the tunnelling correction factor Γ at 298 K.

The total partition functions of reactants and transition states to be used in the rate constant calculation using Eq. (3) were calculated at MPWB1K/6-31+G (d,p) level of theory. The total partition function is approximated by the product of translational, rotational, vibrational, and electronic partition functions. Several low frequency vibrational modes were identified as internal rotations.[31] The total partition function of reactants [CF$_3$C(O)OCH$_2$CF$_3$] and transition states (TS-OH and TS-Cl) were corrected for hindered rotor as given by the following expression

$$Q_{corr} = \frac{Q_{HO} \cdot Q_{IR}}{\Pi_{Q_{v=i}}} \quad (8)$$

where Q_{HO} is the harmonic oscillator partition function, Q_{IR}

the internal rotation partition function and $Q_{v=i}$ is the partition function of normal mode vibrations corresponding to internal rotation.

The electronic partition functions of OH radical and Cl atom were modified to take into account the splitting of their electronic level due to spin-orbit coupling. The ground $^2P_{3/2}$ (with degeneracy of 4) and excited $^2P_{1/2}$ (with degeneracy of 2) states of Cl atom are separated by an energy difference of 881 (cm^{-1}).[32] Thus, Q_{elec} (Cl) is written as

$$Q_{elec} (Cl) = 4 + 2 \exp (-881 \text{ cm}^{-1} \cdot hc/kT) \tag{9}$$

On the other hand, the 4-fold degenerate ground state of OH radical splits up into two doubly degenerate levels separated by an energy difference of 139.7 (cm^{-1}) as given by Ogura *et al.*[33] In such a case Q_{elec} (OH) is given by the expression
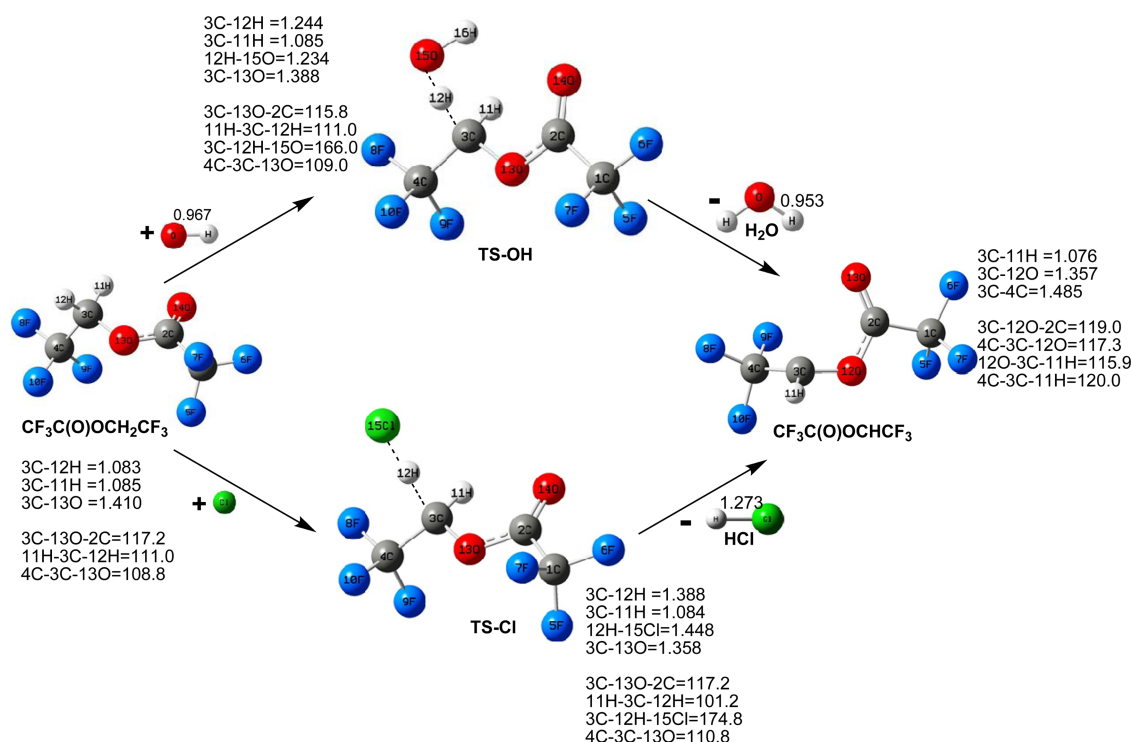
$$Q_{elec} (OH) = 2 + 2 \exp (-139.7 \text{ cm}^{-1} \cdot hc/kT) \tag{10}$$

Results and Discussion

Electronic Structure. The optimized structures of reactants, products and transition states obtained at MPWB1K/6-31+G(d,p) level of theory are shown in Figure 1. The significant structural parameters are also noted along the significant bonds and these are also shown in Figure 1. Transition state (TS-OH) is formed as a result of OH radical attack on the parent molecule. The O atom of the OH radical forms a new O·····H (15O−12H) (refer to Fig. 1 for the numbering on the atom) bond by attaching it with the H

atom of the C-H (3C−12H) bond of the parent molecule. The newly formed O·····H (15O−12H) bond is found to be 1.234 Å which is about 28% larger than the isolated O-H bond distance in H$_2$O molecule calculated to be 0.953 Å. The same observation is true in the case of abstraction of H by Cl atom. In the latter case the breaking C-H bond stretched from 1.083 to 1.388 (~28%) whereas, the forming H-Cl bond in TS-Cl is 1.448 Å which is about 15% larger than that of 1.273 Å in the isolated HCl molecule. The elongation of the breaking bond in the case of TS-Cl may be due to the strong electronegative character of the Cl atom.
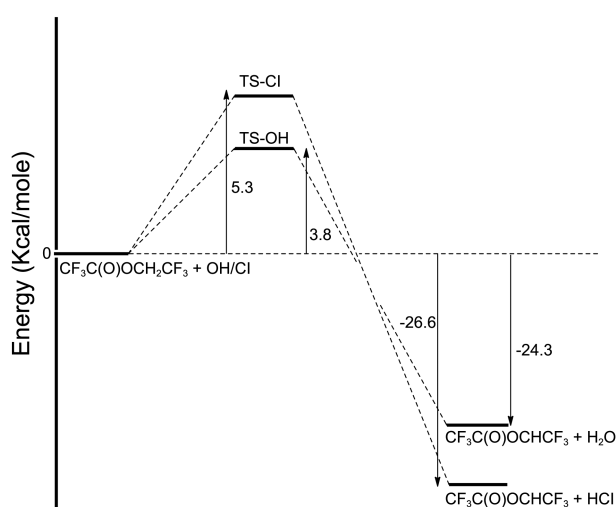
The unscaled vibrational frequencies of the corresponding molecules for reactions 1 and 2 calculated at MPWB1K/6-31+G(d,p) are given in Table 1. The frequencies corresponding to the saddle point on the potential energy surface corresponding to the transition states (TS-OH and TS-Cl) are **1744i** cm^{-1} and **1167i** cm^{-1} respectively. The larger absolute value of the imaginary frequency at 1744 cm^{-1} for H-abstraction by OH radical in reaction channel 1 envisages that the width of the potential barrier might be narrow and the tunnelling effect may be pronounced and should be taken into account during the calculation of the rate constant. For unrestricted calculations spin contamination is the major issue. The spin contamination $\langle S^2 \rangle$ values of all the species involved in reactions 1 and reaction 2 are given in Table 1. The $\langle S^2 \rangle$ values for the doublet vary from 0.752 to 0.761 before annihilation while $\langle S^2 \rangle$ value after annihilation for pure doublet is 0.75. Thus, wave functions were presumed not to be contaminated by states of higher multiplicities. The IRC calculation performed for TS-OH and TS-Cl are shown

Figure 1. Optimized geometries of reactants, products and transition states involved in reaction (1) and (2) obtained at MPWB1K/6-31+G(d,p) level of theory.

Table 1. Unscaled vibrational frequencies of reactants, products and transition states at the MPWB1K/6-31+G(d,p) level of theory

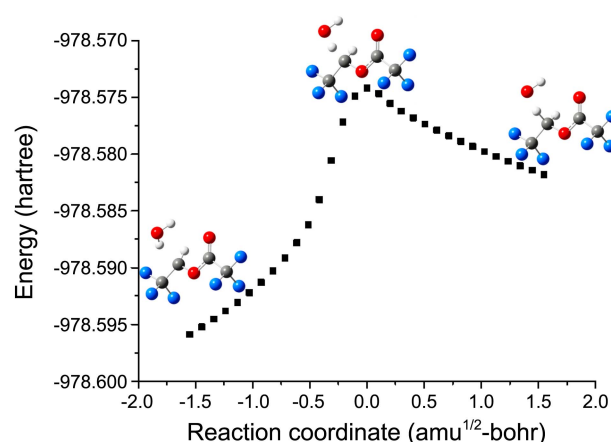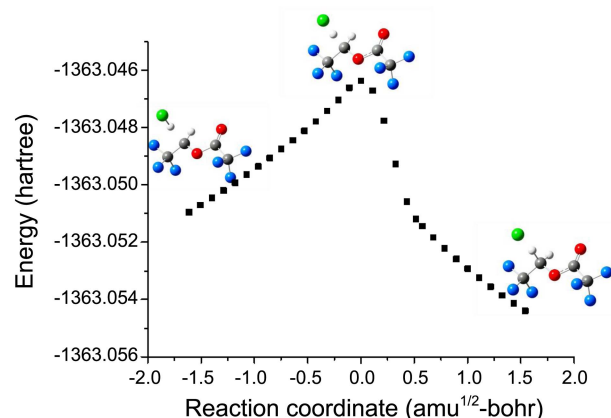| Species	Vibrational frequencies (cm^{-1})	$\langle S^2 \rangle$
$CF_3C(O)OCH_2CF_3$	23, 47, 57 ,65, 173, 204, 267, 293, 340, 387, 424, 473, 533, 540, 562, 610, 688, 759, 807, 873, 895, 1029, 1101, 1221, 1267, 1277, 1279, 1337, 1354, 1382, 1457, 1490, 1516, 1968, 3192, 3268	0.0
OH	3870 (3738)^a	0.752
TS-OH	*1744i*, 19, 46, 55, 84, 177, 200, 251, 286, 327, 335, 358, 420, 459, 481, 535, 551, 570, 619, 693, 767, 807, 877, 887, 966, 1051, 1150, 1197, 1242, 1280, 1285, 1307, 1341, 1352, 1430, 1465, 1505, 1948, 3223, 3882	0.761
TS-Cl	*1167i*, 29, 36, 43, 47, 71, 86, 171, 199, 248, 286, 309, 332, 417, 455, 491, 532, 550, 565, 618, 682, 766, 798, 876, 899, 964, 983, 1147, 1163, 1244, 1271, 1286, 1289, 1347, 1348, 1433, 1472, 1982, 3246	0.759
$CF_3C(O)OCHCF_3$	17, 20, 47, 103, 161, 204, 247, 288, 302, 342, 427, 470, 510, 531, 608,633, 702, 776, 796, 880, 907, 1132, 1195, 1256, 1268, 1277, 1335, 1353, 1436, 1483, 1986, 3328	0.753
HCl	3085 (2991)^a	0.0
H_2O	1637, 3975, 4101 (1595, 3657, 3756)^a	0.0

^{a}Values given in parentheses are the experimental values taken from Ref. 34.

Figure 2. Potential energy diagram for reactions 1 and 2 at G2 (MP2)//MPWB1K/6-31+G(d,p) level of theory. All values are in kcal/mol.

Figure 3. IRC data of TS-OH for the hydrogen abstraction of $CF_3C(O)OCH_2CF_3$ by OH atom calculated at MPWB1K/6-31+G(d,p).

Figure 4. IRC data of TS-Cl for the hydrogen abstraction of $CF_3C(O)OCH_2CF_3$ by Cl atom calculated at MPWB1K/6-31+G(d,p).

in Figures 3 and 4 respectively showing thereby that the transition from reactants to products were smooth through the corresponding transition state.

Rate Constant

The barrier height for reactions 1 and 2 considered during the present study are determined using dual level dynamics method G2(MP2)//MPWB1K/6-31+G(d,p) in which the single point energy calculation is perform at G2(MP2) level on the geometry optimized at MPWB1K/6-31+G(d,p). A potential energy diagram is constructed by plotting zero-point corrected total energy of the species concerned with respect to the reactants arbitrary taken as zero. This is shown in Figure 2. The results show that reaction 2 initiated by Cl atom has a higher energy barrier (5.3 kcal/mol) as compared to reaction 1 initiated by OH (3.8 kcal/mol). This envisages that OH attack for H-abstraction is more favourable than the Cl initiated H-abstraction reaction in reactions with titled molecule.

The rate constants for reactions 1 and 2 are calculated

using canonical transition state theory (CTST). The total partition function of reactant ($CF_3C(O)OCH_2CF_3$) and transition states (TS-OH and TS-Cl) are corrected for hindered rotors. Several low frequencies obtained during vibrational frequency calculation have been found to behave like internal rotors and are taken into consideration during the calculation

Table 2. Total partition function (Q), partition function for internal rotation (Q_{IR}) and corrected partition function ($Q_{corrected}$) for the reactant and transition states at MPWB1K/6-31+G(d,p) level

Species	Q	Q_{IR}	$\prod Q_{v=i}$	$Q_{corrected}$
CF$_3$C(O)OCH$_2$CF$_3$	1.483680×10^{18}	5.338000×10^2	9.676450	8.184700×10^{19}
TS-OH	5.409640×10^{19}	9.383979×10^4	5.588757	9.083176×10^{23}
TS-Cl	1.729900×10^{20}	3.899984×10^4	3.764426	1.792194×10^{23}
OH	6.423280×10^7	–	–	9.067600×10^7
Cl	1.625580×10^7	–	–	1.648730×10^7

of the corrected partition functions. The partition function corresponding to these frequencies were excluded from the normal mode vibrational frequencies of reactant and transition states and the total partition function was corrected using Eq. (8) and used in the rate constant calculation. The corrected partition functions are listed in Table 2. Significantly higher absolute values of the imaginary frequencies obtained at 1744 and 1167 cm^{-1} for TS-OH and TS-Cl respectively show that reaction proceeded with a narrow width and tunnelling may be significant. We utilized Eckart potential for forward and reverse barriers and using the method developed by Brown[29] for the calculation of the tunnelling correction factor. The values come out to be 11.45 and 4.21 for reactions (1) and (2) which is significantly higher than the value calculated by simple Wigner's method (3.9 and 2.1) for respective reactions. Taking into account the corrected partition functions, barrier heights and tunnelling factors, the rate constants for reactions (1) and (2) are calculated using Eq. (3) and have been found to be 5.3×10^{-13} and 2.0×10^{-14} cm^3 molecule^{-1} sec^{-1} respectively. These calculated values are compared with the experimental values determined by Blanco *et al.*[17] based on relative rate method using FTIR detection technique. The calculated rate constants are found to be about 5 and 10 times higher than the experimental value of 1.1×10^{-13} cm^3 molecule^{-1} sec^{-1} and 1.18×10^{-15} cm^3 molecule^{-1} sec^{-1} for reactions 1 and 2 respectively as determined by Blanco *et al.*[17] In another study using the same experimental technique Wallington *et al.*[18] determined the rate constant for reaction 2 as 9.0×10^{-16} cm^3 molecule^{-1} sec^{-1} which is about 20 times lower than the calculated value obtained during the present investigation.

Conclusions

Hydrogen atom abstraction reactions of 2,2,2-trifluoroethyl trifluoroacetate by OH and Cl have been studied at MPWB1K/6-31+G(d,p). Transition states have been characterised and the intrinsic reaction coordinate analysis has been performed on geometry obtained at the same level of theory. Results showed that the transition states connected the reactant and products and the transition was smooth through the transition state. The barrier heights are determined at G2(MP2) level and the partition functions were corrected for internal rotations. These are used in the rate constant calculation based on the canonical transition state theory. Tunnelling corrections are made using one-dimen-

sion Eckart potential. The calculated rate constants are found to be almost 5 to 10 times higher than the experimentally observed values obtained by relative rate methods based on FTIR detection technique.

References

1. Solomon, S. *Nature* **1990**, *6291*, 347.
2. Molina, M. J.; Rowland, F. S. *Nature* **1974**, *249*, 810.
3. Rowland, F. S.; Molina, M. J. *Chem. Eng. News.* **1994**, *72*, 8.
4. Weubbles, D. J. *J. Geophys. Res.* **1983**, *88*, 1433.
5. Ravishankara, R. A.; Turnipseed, A. A.; Jensen, N. R.; Barone, S.; Mills, M.; Howard, C. J.; Solomon, S. *Science* **1994**, *263*, 71.
6. Imasu, R.; Suga, A.; Matsuno, T. *J. Meteorol Soc. Jpn.* **1995**, *73*, 1123.
7. Houghton, J. T. *et al.* The Scientific Basis, Contribution of Working Group I to the Third Assessment Report of the Intergovernmental Panel on Climate Change, (IPCC), Geneva, 2001.
8. Blanco, M. B.; Bejan, I.; Barnes, I.; Wiesen, P.; Truel, M. *Environmental Science & Technology* **2010**, *44*, 2354.
9. Oyaro, N.; Sellevag, S. R.; Nielsen, C. J. *Environmental Science & Technology* **2004**, *38*, 5567.
10. Ninomiya, Y.; Kawasaki, M.; Guschin, A.; Molina, L. T.; Molina, M. J.; Wallington, T. J. *Environmental Science & Technology* **2000**, *34*, 2973.
11. Christensen, L. K.; Wallington, T. J.; Guschin, A.; Hurley, M. D. *J. Phys. Chem. A* **1999**, *103*, 4202.
12. Wallington, T. J.; Schneider, W. F.; Sehested, J.; Bilde, M.; Platz, J.; Nielsen, O. J.; Christensen, L. K.; Molina, M. J.; Molina, L. T.; Wooldridge, P. W. *J. Phys. Chem. A* **1997**, *101*, 8264.
13. Finlayson-Pitts, B. J.; Pitts, J. N., Jr. *Atmospheric Chemistry*; Wiley: New York, 1986.
14. Mellouki, A.; Le Bras, G.; Sidebottom, H. *Chemical Review* **2003**, *103*, 5077.
15. Wallington, T. J.; Hurley, M. D.; Fedotov, V.; Morrell, C.; Hancock, G. *J. Phys. Chem. A* **2002**, *106*, 8391.
16. Nohara, K.; Toma, M.; Kutsuna, S.; Takeuchi, K.; Ibusuki, T. *Environmental Science & Technology* **2001**, *35*, 114.
17. Blanco, M. B.; Teruel, M. A. *Atmospheric Environment* **2007**, *41*, 7330.
18. Wallington, T. J.; Guschin, A.; Stein, T. N. N.; Platz, J.; Sehested, J.; Christensen, L. K.; Nielsen, O. J. *J. Phys. Chem. A* **1998**, *102*, 11152.
19. Frisch, M. J. *et al Gaussian09* (Version C.01), 2010, Gaussian, Inc, Wallingford, CT.
20. Zhao, Y.; Truhlar, D. G. *J. Phys. Chem. A* **2004**, *108*, 6908.
21. Perdew, J. P. Unified theory of exchange and correlation beyond the local density approximation. In: *Electronic Structure of Solids*, Ziesche, P., Eschrig, H., Eds.; Akademie Verlag: Berlin, 11-20.
22. Becke, A. D. *J. Chem. Phys.* **1996**, *104*, 1040.

23. Zhao, Y.; Schultz, N. E.; Truhlar, D. G. *J. Chem. Theor. Comput.* **2006**, *2*, 364.

24. Curtiss, L. A.; Raghavachari, K.; Pople, J. A. *J. Chem. Phys.* **1993**, *98*, 1293.

25. Scott, A. P.; Radom, L. *J. Phys. Chem.* **1996**, *100*, 16502.

26. Truhlar, D. G.; Garrett, B. C.; Klippenstein, S. J. *J. Phys. Chem.* **1996**, *100*, 12771.

27. Johnston, H. S. *Gas Phase Reaction Rate Theory*; Ronald Press: New York, 1966; p 362.

28. Eckart, C. *Phys. Rev.* **1930**, *35*, 1303.

29. Brown, R. L. *J. Res. Natl. Bur. Stand.* **1981**, *86*, 357.

30. Johnston, H. S.; Heicklen, J. *J. Phys. Chem.* **1962**, *66*, 532.

31. Chuang, Y. Y.; Truhlar, D. G. *J. Chem. Phys.* **2000**, *112*, 1221.

32. Chase, M. W., Jr.; Davies, C. A.; Downey, J. R., Jr.; Frurip, D. J.; McDonald, R. A.; Syverud, A. N. *Phys. Chem. Ref. Data* **1985**, 14, Suppl 1, 3rd edn.

33. Ogura, T.; Miyoshi, A.; Koshi, M. *Phys. Chem. Chem. Phys.* **2007**, *9*, 5133.

34. NIST Computational Chemistry Comparison and Benchmark Database, NIST Standard Reference Database 101, Release 15b, August 2011, Johnson, Russel, D., Ed.; http://cccbdb.nist.gov/.